Direct numerical simulation of supersonic cavity-based premixed flame stabilization: Effect of inflow turbulence

Minqi Lin[a], Jian Fang[b], Xi Deng[c], Zhi X. Chen[a,d,*]
[a] State Key Laboratory of Turbulence and Complex Systems, Peking University
Beijing, China
[b] Scientific Computing Department, Science and Technology Facilities Council (STFC),
Daresbury Laboratory, Warrington, United Kingdom
[c] Department of Engineering, University of Cambridge
Cambridge, United Kingdom
[d] AI for Science Institute (AISI), Beijing
Beijing, China

1 Introduction

For the air-breathing scramjets, stabilizing flame is an important issue because of the relatively large Mach number inside the combustor, resulting in a short residence time for the mixture to ignite and propagate [1]. Wall cavity therefore adopted as a proven effective approach to provide a low-speed region with vortices [2] forming an ideal zone for flame-holding to achieve sustainable combustion. To further enhance the stabilization of supersonic combustion, different geometries of cavity (such as angled rear-wall) have been proposed [3] and various numerical studies were carried out to understand the fuel-mixing and combustion processes as reviewed in [4]. Among the different fuels for combustion, hydrogen has been most widely studied due to its high chemical reactivity. Kim et al. [5] studied upstream injection with supersonic inflow condition. Recently, Sitaraman et al. [6] compared two cases with different injection positions on the bottom wall of the cavity. Adaptive mesh refinement was used for higher numerical accuracy particularly near the shock waves. However, among the previous numerical works on cavity-based (perhaps in general) supersonic combustion, high-order direct numerical simulation (DNS) is rarely used due to high computational cost and stringent requirements for the numerical schemes. Aditya et al. [7] performed the DNS of a turbulent premixed ethylene-air flame over a backward-facing step using the well-known S3D code, which is eighth-order in space and fourth-order in time. Using the same code, Rauch et al. [8] presented a two-dimensional DNS investigation of premixed turbulent flame with rectangular and linear ramp cavity to make comparison, showing the better entry of fuel into cavity by linear ramp cavity. However, both of these studies were carried out under subsonic inflow conditions.

In this work, we present a DNS study of the supersonic premixed combustion in a model scramjet combustor. This configuration with a free stream Mach number of 1.5 is similar to the dual-mode, direct-connect combustor at the University of Virginia Supersonic Combustion Facility [9]. Instead of

Correspondence to: chenzhi@pku.edu.cn

the direct injection of fuel, premixed hydrogen/air mixture is considered. Inlet turbulence, is included via a precursor channel flow DNS to minic the fully developed supersnoic duct flow upstream of the combustor in the experiments. To find the effect of inflow turbulence, We present time-averaged profile of duck flow as inlet boundary condition to make primary comparison between two cases.

2 Simulation Details

The three-dimensional compressible Navier-Stokes (N-S) equations are solved in the DNS. Considering multi-species chemical reaction, the governing equations are written as

$$\frac{\partial \rho}{\partial t} + \frac{\partial \rho u_i}{\partial x_i} = 0 \,, \tag{1}$$

$$\frac{\partial \rho u_i}{\partial t} + \frac{\partial \rho u_i u_j}{\partial x_j} = -\frac{\partial p}{\partial x_i} + \frac{\partial \sigma_{ij}}{\partial x_j} \,, \tag{2}$$

$$\frac{\partial \rho e}{\partial t} + \frac{\partial (\rho e + p) u_i}{\partial x_i} = -\frac{\partial q_i}{\partial x_i} + \frac{\partial \sigma_{ij} u_i}{\partial x_j} \,, \tag{3}$$

$$\frac{\partial \rho Y_k}{\partial t} + \frac{\partial \rho Y_k (u_i + V_{k,i})}{\partial x_i} = \dot{\omega}_k \tag{4}$$

where ρ is the density, u_i is the velocity component in i direction, p is the pressure, e is the total energy per unit mass. Y_k, D_k and $\dot{\omega}_k$ represent the mass fraction, coefficient of mass diffusion and mass based chemical source term of the kth species respectively. The diffusion velocity is $V_{k,i} = -\frac{1}{X_k} D_k \frac{\partial X_k}{\partial x_i} + \sum_k \frac{Y_k}{X_k} D_k \frac{\partial X_k}{\partial x_i}$, where D_k is the mixture-averaged diffusion coefficient and thermal diffusion is neglected in this work. The stress tensor and heat flux vector are denoted by σ_{ij} and q_i.

A finite difference method is adapted to solve the transport equations. An in-house high-order computational fluid dynamics code, ASTR, which has already been applied to a series of previous simulations [10–14], is used for this study. The code is coupled with Cantera's Fortran interface to calculate chemical kinetics and transport properties. The convection terms of Eq. (1) $\sim$ (4) are approximated by a seventh-order low-dissipative monotonicity-preserving scheme [15] in order to preserve accuracy near shock-waves. As for diffusion terms, sixth-order central scheme is adapted. The temporal integration is conducted by a three-step third-order Runge-Kutta method.

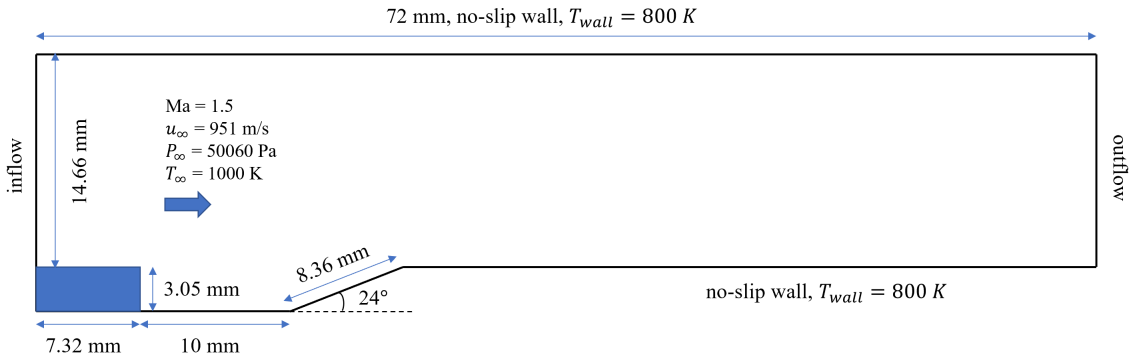

Figure 1: x-y plane of computation domain and condition.

The computational domain is set to be a quasi-3D planar channel with a cavity embedded in the lower wall. The size of computational domain and boundary conditions are marked in Figure 1. Non-slip wall

boundary with fixed wall temperature is applied to the top and bottom wall to avoid premature auto-ignition in the jet flow and a simple outflow condition is applied to the supersonic outlet. The depth in spanwise direction is 6 mm and periodic condition is set on the two boundaries. Immersed boundary method, presented by Vanna et al. [16] with some modifications, is used for the upstream wall and front wall of the cavity, and the boundary conditions of those two walls are set to be consistent with bottom wall. The domain is discretized with a 1450×320×200 mesh in streamwise, wall-normal and spanwise direction. The mesh is smoothly deformed according to the change of the domain geometry and finer mesh is used along boundary layer. To validate the mesh, we calculate parameters at the inlet plane boundary layer. Details are listed in Table 1.

Table 1: Mesh validation at the inlet plane.

$\Delta x/\eta_1$	$\Delta y/\eta_1$	$\Delta z/\eta_1$	$\Delta e/\eta_1$	$\Delta x/\eta_e$	$\Delta y/\eta_e$	$\Delta z/\eta_e$	$\Delta e/\eta_e$
7.69	0.60	4.51	2.75	1.78	2.61	1.04	1.69

The subscript '1' stands for the value at the wall considering the surface of immersed boundary and the subscript 'e' represent the value at the edge of boundary layer. The effective mesh size Δe is defined as $\Delta e = \sqrt[3]{\Delta x \Delta y \Delta z}$.

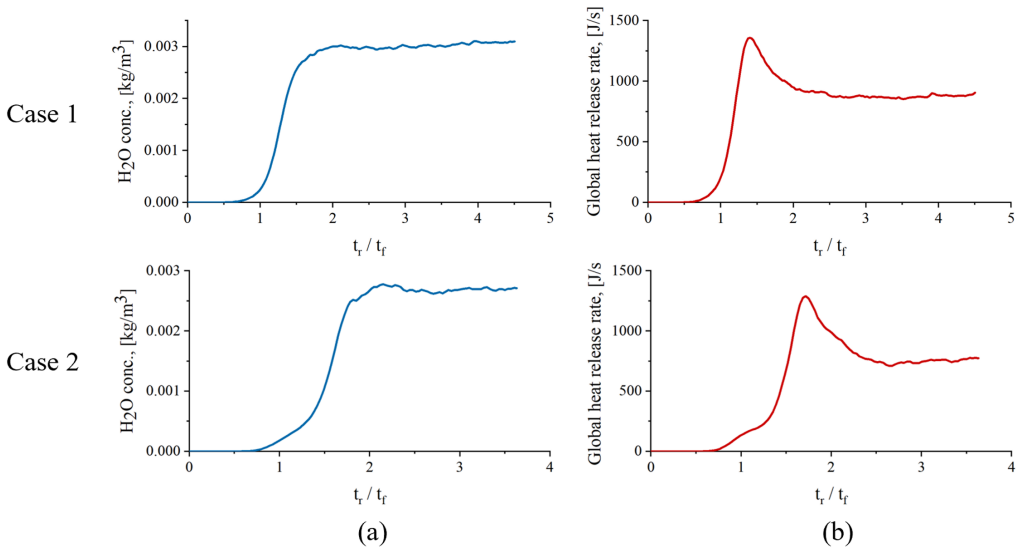

Figure 2: Volume-based value over the area near the cavity: (a) averaged H_2O concentration; (b) integrated heat release rate. One flow-though-time $t_f = 7.57 \times 10^{-5}$ s, t_r is the physical time counted since the reactant added in the domain.

The simulation is first initialised with a non-reacting solution obtained from 2D simulation with a laminar inflow. To obtain inflow data for inlet plane, we conducted a precursor channel flow DNS [14], using a steady wall blowing and suction to trigger a boundary layer transition. Then a series of inflow slices were preserved from the fully developed turbulent zone in the channel as primary inflow data. After decomposing the turbulent data into mean flow and fluctuations, the mean boundary layer profiles were utilized for the laminar inlet condition (Case 2). To obtain turbulent inlet condition (Case 1), uncorrelated fluctuations from two instants were mapped to upper and lower boundary layers respectively. The temporal inflow fluctuations were updated with the simulation using a cubic spline interpolation. Therefore the nominal thickness of boundary layer is $\delta_0 = 1.47$ mm and corresponding Reynolds number for inlet flow is Re_{δ_0}=5187. After setting up the cases, we let the simulation evolved for at least one flow-through time to eliminate the effect of initialisation. With the reactant added in the domain, the

solution is evolved for more than three flow-through times. To analysis combustion in region near the cavity, we refer an area with length of 4.5 cm along x-direction and height of 0.8 cm along y-direction as the *near-cavity area* hereafter. Figure 2 shows the volume-averaged value of H_2O mass concentration and integrated heat release over this area, indicating that combustion of both two cases can reach a statistically stationary state in near-cavity area after about 2.5 flow-through time. A typical reacting flow simulation of 5 flow-through-times requires a wall-clock time of about 1.5 days on 16384 processors.

3 Result and Discussion

After several prior simulations, the equivalence ratio $\phi = 0.3$ is used and combustion near the cavity can reach a statistically stationary burning state. Figure 3 presents a typical 3D view of the flow field in the near cavity region. It is seen that the heat release iso-surface lies within the cavity shear layer and extends downstream along the bottom wall. Inside the cavity, however, heat release only takes place near the rear ramp with a higher temperature.

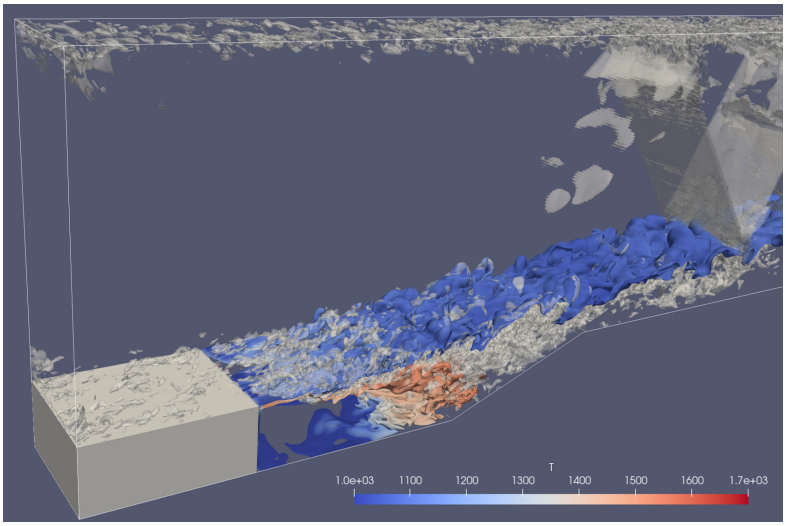

Figure 3: Typical 3D view of heat release rate and pressure gradient $|\nabla p|$ iso-surfaces for Case 1. Heat release rate is contoured at the value of 5×10^8 J/m^3/s, colored by temperature. $|\nabla p|$ is contoured at the value of 2×10^7 Pa/m.

The instant flow field on x-y plane in the middle of spanwise direction is shown in Figure 4, giving an overall comparison between the cases with and without inflow turbulence (IT). It can be observed that inlet turbulence leads to more vortices in the cavity and the shear layer turbulence develops significantly faster above the cavity in Case 1. Also, Figure 4 shows that inflow turbulence strongly influences the mixture temperature inside the cavity resulting in lower values everywhere but above the aft wall. Since the overall heat release rate for Case 1 is higher in Figure 2(b), the lower temperature is possibly due to the higher heat loss induced by the inflow turbulence.

Since HO_2 radical is commonly used as flame reaction zone marker, the contour plot of HO_2 mass fraction is carried out to compare the flame location between two cases. As the result shown in Figure 5(a), the contour line is more curled in Case 1 because of vortices in cavity shear layer and area near aft wall, which represents thicker reaction zone and larger flame surface. This can further indicate more efficient combustion in shear layer with inflow turbulence. In addition, the distribution of H_2 in Figure 5(b) shows the ability of fresh mixture to enter the shear layer and cavity. With inlet turbulence, we can see more reactants flow into the thicker reactive area and offer proper condition for sustainable combustion.

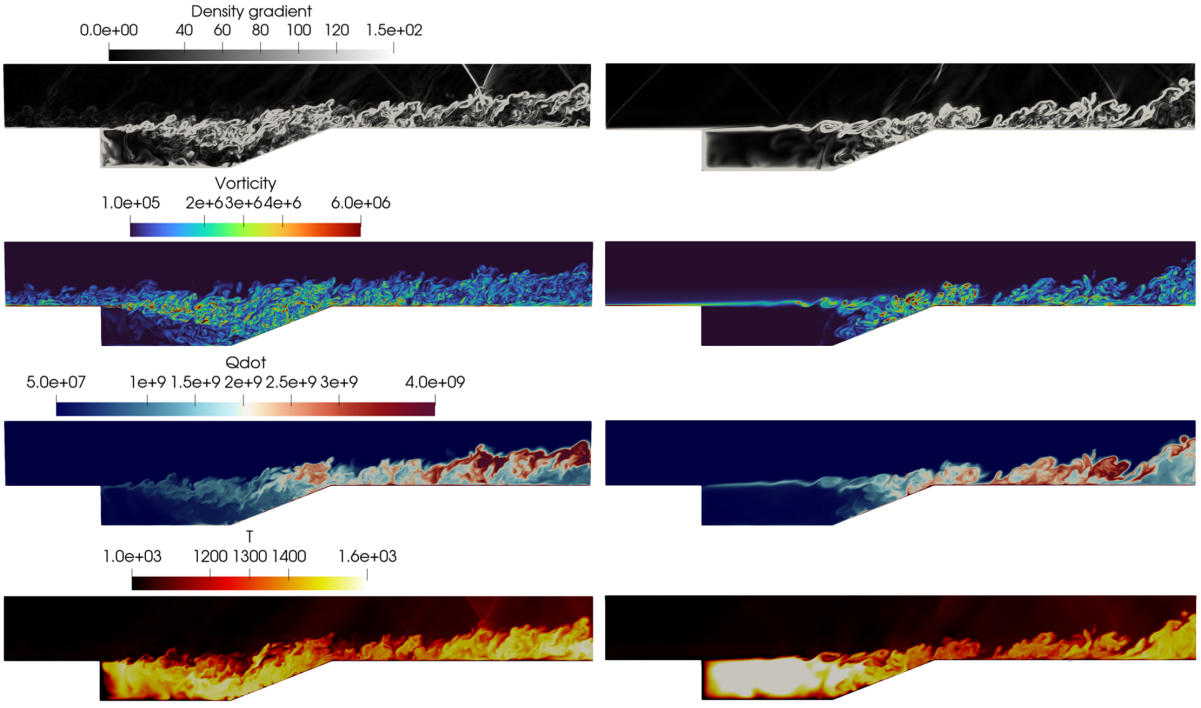

Figure 4: The instantaneous field of near-cavity area in x-y plane. From top to bottom is density gradient $|\nabla\rho|$ [kg/m^4], Vorticity $|\nabla \times \vec{u}|$ [1/s], heat release rate [J/m^3/s], temperature [K]. (a) Case 1 with IT; (b) Case 2 without IT.

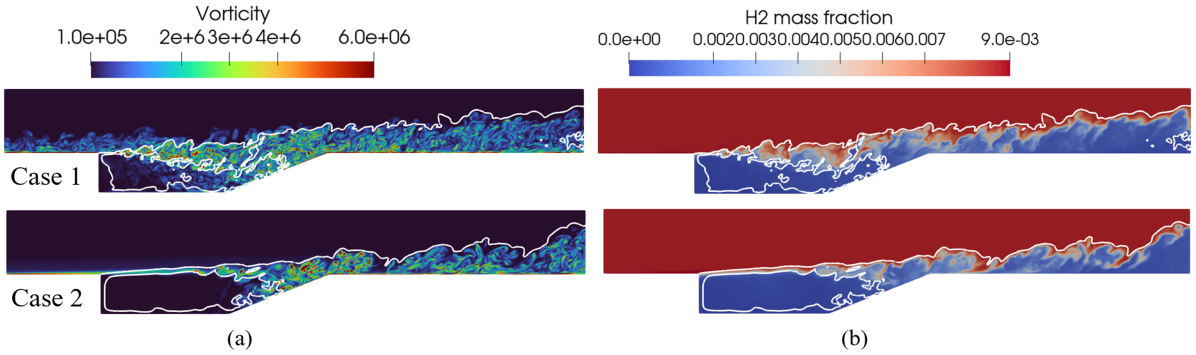

Figure 5: Snapshot of near-cavity area in x-y plane. (a) Vorticity $|\nabla \times \vec{u}|$ [1/s]; (b) mass fraction of H_2. White line is a contour line of $Y_{HO_2} = 4 \times 10^{-5}$.

4 Conclusion

Direct numerical simulation of premixed turbulent hydrogen/air flame over a cavity was performed to understand the flame stabilization under a supersonic inflow condition. Two DNS cases with turbulent and laminar inlet conditions were carried out to learn the effect of inflow turbulence. The results show that with turbulent inflow flame surface was enlarged and curled because of strengthened vortices in the shear layer above the cavity, which indicates more robust and effective combustion. However, the stronger shear turbulence was found to increase the wall heat loss around the cavity leading to generally lower temperatures. The role of the shear-induced oblique shock is yet unclear and further analysis is required to shed light into the flame stabilisation mechanism in this type of configurations.

References

[1] Urzay J. (2018). Supersonic combustion in air-breathing propulsion systems for hypersonic flight. Annu. Rev. Fluid Mech. 50:593–627.

[2] Gruber MR, Baurle RA, Mathur T, Hsu K-Y. (2001). Fundamental studies of cavity-based flameholder concepts for supersonic combustors. J. Propuls. Power. 17(1):146–153.

[3] Sun M, Wang H, Cai Z, Zhu J. (2020). Unsteady supersonic combustion. Springer.

[4] Barnes FW, Segal C. (2015). Cavity-based flameholding for chemically-reacting supersonic flows. Prog. Aerosp. Sci. 76:24–41.

[5] Kim KM, Baek SW, Han CY. (2004). Numerical study on supersonic combustion with cavity-based fuel injection. Int. J. Heat Mass Transf. 47(2):271–286.

[6] Sitaraman H, Yellapantula S, Henry de Frahan MT, Perry B, Rood J, Grout R, Day M. (2021). Adaptive mesh based combustion simulations of direct fuel injection effects in a supersonic cavity flame-holder. Combust. Flame. 232:111531.

[7] Aditya K, Kolla H, Chen JH. (2019). DNS of a turbulent premixed flame stabilized over a backward facing step, in: 11th US National Combustion Meeting.

[8] Rauch AH, Konduri A, Chen J, Kolla H, Chelliah HK. (2018). DNS investigation of cavity stabilized premixed turbulent ethylene-air flame, in: 2018 AIAA Aerospace Sciences Meeting, p. 1674.

[9] Cutler AD, Gallo EC, Cantu LM, Rockwell RD, Goyne CP. (2018). Coherent anti-stokes raman spectroscopy of a premixed ethylene–air flame in a dual-mode scramjet. Combust. Flame. 189:92–105.

[10] Fang J, Yao Y, Li Z, Lu L. (2014). Investigation of low-dissipation monotonicity-preserving scheme for direct numerical simulation of compressible turbulent flows, Comput. Fluids. 104:55–72.

[11] Fang J, Yao Y, Zheltovodov AA, Li Z, Lu L. (2015). Direct numerical simulation of supersonic turbulent flows around a tandem expansion-compression corner. Phys. Fluids. 27(12):125104.

[12] Fang J, Yao Y, Zheltovodov AA, Lu L. (2017). Investigation of three-dimensional shock wave/turbulent-boundary-layer interaction initiated by a single fin. AIAA J. 55(2):509–523.

[13] Fang J, Zheltovodov AA, Yao Y, Moulinec C, Emerson DR. (2020). On the turbulence amplification in shock-wave/turbulent boundary layer interaction. J. Fluid Mech. 897:A32.

[14] Fang J, Deng X, Chen ZX. (2023). Direct numerical simulation of supersonic internal flow in a model scramjet combustor under a non-reactive condition. Phys. Fluids. 35:026103.

[15] Fang J, Li Z, Lu L. (2013). An optimized low-dissipation monotonicity-preserving scheme for numerical simulations of high-speed turbulent flows. J. Sci. Comput. 56:67–95.

[16] De Vanna F, Picano F, Benini E. (2020). A sharp-interface immersed boundary method for moving objects in compressible viscous flows. Comput Fluids. 201:104415.